Smart Structures and Systems, *Vol. 25, No. 3 (2020) 279-284*
DOI: https://doi.org/10.12989/sss.2020.25.3.279

Study on magnetorheological damper stiffness shift

Mohammad H. Jafarkarimi [a], Shahryar Ghorbanirezaei [b], Yousef Hojjat* and Vahid Sabermand [c]

Department of Mechanical Engineering, Tarbiat Modares University, Jalal Ale Ahmad, No. 7, Iran

(*Received November 5, 2018, Revised October 28, 2019, Accepted February 17, 2020*)

Abstract. Electrical current is usually used to change the damping force of Magnetorheological Dampers (MRDs). However, changing the electrical current could shift the stiffness of the system, the phenomenon that was not considered carefully. This study aims to evaluate this shift. A typical MRD was designed, optimized, and fabricated to do some accurate and detailed experimental tests to examine the stiffness variation. The damper is equipped with a circulating system to prevent the deposition of particles when it is at rest. Besides that, a vibration setup was developed for the experimental study. It is capable of generating vibration with either constant frequency or frequency sweep and measure the amplitude of vibration. The damper was tested by the vibrating setup, and it was concluded that with a change in electrical current from 0 to 1.4 A, resonant frequency would change from 13.8 Hz to 16 Hz. Considering the unchanging mass of 85.1 kg, the change in resonant frequency translates as a shift in stiffness, which changes from 640 kN/m to 860 kN/m.

Keywords: magnetorheological damper; stiffness shift; magnetorheological fluid; magnetorheological valve

1. Introduction

Dampers as shock absorbers are the heart of vibrating systems and play significant roles in the control of unwanted vibrations and forces. Two types of smartly tuned mass damper were theoretically and experimentally studied by Sun *et al.* (2014a). They found displacement and acceleration transfer functions and closed-form expressions to prove that the structural responses to harmonic excitations and ground motions would decrease substantially. Practical guidelines for active controlling and band-pass filtering of vertical vibrations of bridges, based on tuning of direct velocity feedback control and consideration of maximum damping performance, was non-dimensionally and experimentally studied by Wang *et al.* (2018). In recent years, the progress of Magnetorheological (MR) has produced the desired results of modifying and developing electromagnetic dampers. Being controllable, having immediate responses, and experiencing different viscosity when working, are the benefits of semi-active MR dampers (MRDs), especially in buildings that experience seismic responses because of earthquakes. For protection in such loading conditions, Askari *et al.* (2016) used acceleration feedback to put forward new TSKFInv and MaxMin algorithms for controlling the MRDs of tall buildings.

Varying stiffness to have better control over vibrations seems a popular area of research. Variable stiffness MR-based elastomer for active control of earthquake vibration was studied by Behrooz *et al.* (2014) and Deng *et al.* (2006). In these two studies, a change in natural frequency occurred that meant a stiffness variation. They had to modify the traditional steel–rubber material. In addition to modifying materials, controlling the MR valve was another method to find continuous variable stiffness MRD, which was practiced by Li *et al.* (2009). They aimed to design an MRD to absorb the vibrations efficiently by controlling the valve.

A compact MRD that its stiffness and damping properties were variable and controllable was developed by Sun *et al.* (2015). They theoretically and experimentally found the graph of force-displacement in different electrical currents. Since the stiffness of the spring was constant, a change in damping and stiffness was interconnected. However, an extra spring was needed. Maddah *et al.* (2017) reported a decrease (12%) in the stiffness of an MRD when adding an Eddy Current Damper (ECD) and forming a hybrid MRD and ECD. Weber *et al.* (2010) proposed a new damper that its stiffness could be adjusted through changing frequencies of a target structure. The damper was able to emulate controlled stiffness, and thus, it had an adjustable and varying stiffness. Zhu *et al.* (2019) developed a variable stiffness MRD, which was able to harvest power by 2.595 W. When the current changed from 0 to 2 A, the stiffness shifted 70.4%. However, there were two extra springs added to the damper, and they did not study the inherent change in the stiffness of MRD without any springs. Liu *et al.* (2006) proposed a variable stiffness system that included two MRD in series. They changed the configuration of MRD to reach to a variable stiffness MRD.

Variable stiffness MRD also was designed for comfort in vehicles by greatly reducing and controlling the

*Corresponding author, Ph.D., Professor,
E-mail: yhojjat@modares.ac.ir;
Shahryar.ghorbani@modares.ac.ir
[a] M.Sc.
[b] M.Sc.
[c] M.Sc.

http://www.techno-press.org/?journal=sss&subpage=7 ISSN: 1738-1584 (Print), 1738-1991 (Online)

vibrations. Regarding this, Sun *et al*. (2017) developed an advanced MRD, and then successfully tested and evaluated a quarter-car model with the MRD. However, they embedded two external springs. Using quite similar principles of varying stiffness method, Jugulkar *et al*. (2016) developed a consistent MRD for bearing varying weights of passengers in vehicles. In combination with air springs, Sun *et al*. (2014b) proposed a variable stiffness MRD, embedded it in high-speed trains, and compared its dynamic performance with two other existing fixed-stiffness suspension systems. They found it would have better vibration isolation.

One method to alter damping force in semi-active dampers is altering the viscosity of MR fluid by changing electrical current. Changing the electrical current could bring some other shifts; in particular, a variation in stiffness, that is examined in this paper since the inherent MRD stiffness variation was not considered in previous studies. In this regard, most of the previous studies focused on adding extra components to MRDs to find variable stiffness methods without considering the inherent stiffness shift. The contribution of adding those components and the inherent behavior of MR should have exactly addressed in those studies. This is an open question for our future studies. Considering this intrinsic stiffness shift provides engineers with more efficient methods of vibration suppression when designing MRDs for different devices.

In this study, to carry out an accurate evaluation of inherent stiffness change, an MRD without any attachments like springs is designed correctly, optimized, and fabricated. Without optimization, the examination on the stiffness shift might be inaccurate. The resonant frequency would change with increasing electrical currents. Because the mass of the system is constant, any change in resonant frequency translates as a change in stiffness.

2. Design, optimization and fabrication of MRD

Electrical current is usually altered to change viscosity and thus damping force of MRDs. Any changes in electrical current could reform other characteristics of MRDs. In this study, the main focus is examination on switching the stiffness as a result of a change in electrical current. Fig. 1 shows a typical double-ended MRD. To carefully examine a shift in stiffness as a function of this electrical current, an MRD was designed, optimized, and fabricated. The lines below shed more light on the issue put forward.

Since yield stress is directly related to the applied field in activation region, finding a magnetic force in the annular gap is essential to evaluate damping force, valve ratio, and inductive time constant. Some assumptions are required to ease calculations when analytically examining magnetic circuits in a complex geometric such as the valve of MRD. These assumptions may give inaccurate equations. Thus, Maxwell software was utilized to analyze the MR valve numerically. The 2D model was applied because the MR valve was axisymmetric. Simulation aims to identify relationships between changes in the geometry of MR valve and magnetic flux density (B) and magnetic field intensity (H) when flowing electrical current-in other words,

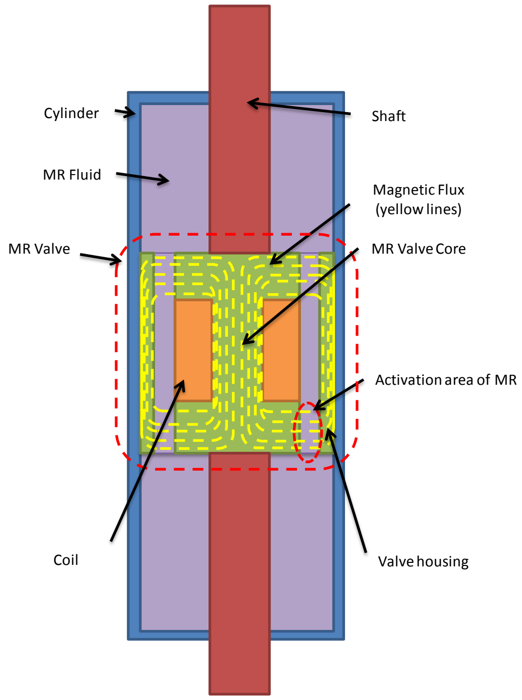

Fig. 1 Cross-section of a double-ended MRD

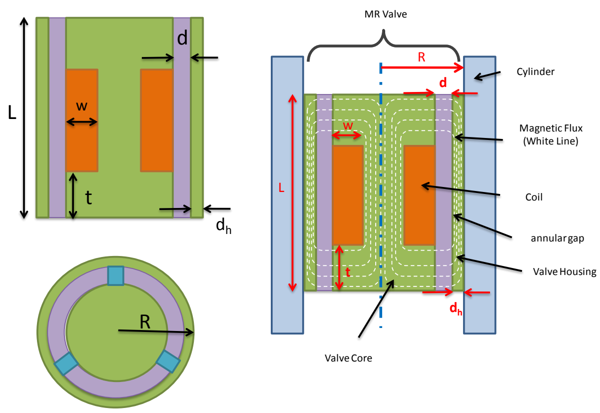

Fig. 2 Geometric parameters

two functions that describe B and H according to geometric parameters. Fig. 2 shows geometric parameters.

Without damaging the test and results, in this study, the length (L) and radius (R) of the MR valve were fixed on 40 mm and 20 mm, respectively, and some ranges of design parameters were considered as Table 1 shows.

Because B and H would change through length of activation region, an imaginary line was assumed at the midpoint of the annular gap in activation region, and the average amount of B and H would be calculated through this line. From Kirchoff law, the conclusion can be made that the relationship between electrical current and magnetic field intensity would be linear. Thus, optimization results for one particular electrical current would be valid for all electrical currents.

In this model, valve housing and valve core were made from pure steel, which were annealed, with a relative permeability of 4000, a coil of copper with a relative

Table 1 Design parameters intervals

Geometric parameter	Interval (mm)
MR valve annular gap	0.8 < d < 1.2
MR valve housing thickness	4< dh < 7
Pole length of MR valve	8 < t < 16
Coil width	3 < w < 9

Table 2 The optimized values of dimensions of Table 1

Parameter	Optimized values (mm)
MR valve annular gap (d)	0.8
MR valve housing thickness (d_h)	5.1
Pole length of MR valve (t)	15.85
Coil width (w)	6.2

permeability of 1 and liquid of Rheological Fluid (MRF-122EG) were chosen. Liquid characteristics were obtained from the product catalog and were given to Maxwell software manually.

The equivalent relations 1 and 2 would be obtained by calculating the areas under the graph of magnetic field intensity versus length of activation region, and magnetic flux density versus length of activation region, divided by the length of activation region. The presented results in Fig. 3, is for a chosen class of design variables that is simulated in COMSOL software. For all other classes, different B and H were found and simulated. The amount of B and H will be estimated among all length of activation region. B_{mr} is magnetic flux density in activation area and H_{mr} is magnetic field intensity in activation area. They are as continuous functions based on these different classes of design variables.

$$B_{mr} = \frac{\int_0^t B_{mr}(s)ds}{t} \tag{1}$$

$$H_{mr} = \frac{\int_0^t H_{mr}(s)ds}{t} \tag{2}$$

Non-linear regression was applied to optimize and present analytic equations. Thus, analytical and continuous functions of obtained results from finite element (B or H) should be found. Minitab software was exploited to achieve this aim. The final continuous equations for B and H become

$$\begin{aligned}\boldsymbol{B} = {} & 0.53233 - 719.929d + 202244d^2 + 53.5859d_h \\ & -3032.34{d_h}^2 - 9998.47d_h d - 13.2608t \\ & -1121.36t^2 + 149.968w - 2201.31w^2 \\ & -3699.76wt + 22271.9dt - 28205dw \\ & -181.36td_h + 545.125d_h w\end{aligned} \tag{3}$$

$$\begin{aligned}\boldsymbol{H} = {} & 239.17 - 441706d + 1.33714e + 008d^2 \\ & +27926.5d_h - 1.34066e + 006{d_h}^2 \\ & -7.14899e + 006d_h d - 18832.5t \\ & +125798t^2 + 82470.1w + 95946.3w^2 \\ & -3.22513e + 006wt + 1.86671e + 007dt \\ & -2.39571e + 007dw - 408529td_h \\ & +664649d_h w\end{aligned} \tag{4}$$

Where d, d_h, t, and w are introduced in Fig. 2 and Table 1.

Objective function (OBJ) should be written according to performance indicators as follows

$$OBJ = \alpha_F \frac{F_{MR,r}}{F_{MR}} + \alpha_d \frac{\lambda}{\lambda_r} + \alpha_T \frac{T}{T_r} \tag{5}$$

Where T, λ and $F_{MR,r}$ are inductive time constant, the ratio of the valve, and damping force, respectively.

F_{MR}, λ_r and T_r are practical reference indicators. According to applications of the damper, which was designed to carry out some experimental tests to evaluate stiffness shift, the values of weighted coefficients of objective function (T, λ and $F_{MR,r}$) were found as $\alpha_F = 0.5\,; \alpha_T = 0.5\,; \alpha_d = 0$.

One of the constrains for the optimization problem was the limitation of geometry dimensions based on the constrained volume of problem. The other one was the value of magnetic flux density, which should be lower than the amount in which MR material saturated because the operational range would be narrower in case the MR was saturated. Based on analysis, magnetic flux was lower than 1 T at the best state. According to the graphs of MRF-122EG material, which shows that the magnetic flux density was 0.33 T in saturation point, it was possible to ignore the last constrain in optimization problem. The reason is that, in practice, the saturation of MRF-122EG fluid would not happen in currents lower than 2 A.

The optimal values of design variables were calculated using the genetic algorithm. The optimization tool of MATLAB software was applied to do this. Table 2 shows the final values.

Eventually, having optimized dimensions from Table 2 - these geometric dimensions are shown in Fig. 2- the MRD was fabricated, and Fig. 4(a) shows the fabricated damper. Both valve core and valve housing that are shown in Fig. 14.b are made from pure iron. After machining with considering optimized geometrical dimensions, both of them were annealed for removing the effect of heat on the valve housing and valve core produced through the machining process. Moreover, because pure iron has high relative permeability and close hysteresis, it was chosen as the material of valve core and valve housing. Fitting the valve housing and valve core needed precision assembly because the annular gap must have a constant width. In other words, the valve core and valve housing must be concentric so that the force applied on the valve would be axial symmetry as Fig. 4(b) shows. As Fig. 14(a) shows, a valve circulates the MR fluid from one side to another. If the MR had not been circulating, MR particles could settle and go down after minutes and could bring some errors when calculating stiffness.

3. Evaluation of MRD stiffness shift

In this study, to evaluate stiffness shift, resonant frequency was carefully examined because the mass of the system was unchanged, any changes in resonant frequency

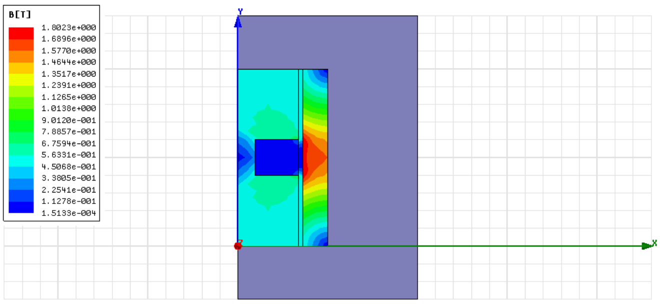

(a) Magnetic field intensity

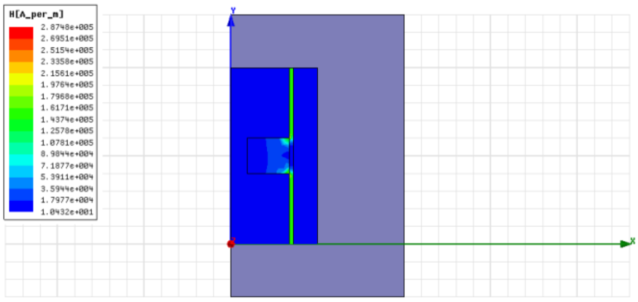

(b) Magnetic flux density for a typical class of design variables

Fig. 3 The obtained results for (a) Magnetic field intensity; (b) Magnetic flux density for a typical class of design variables

(a) Fabricated damper

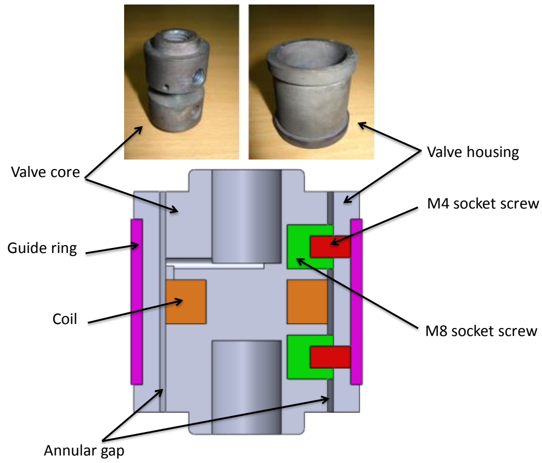

(b) Assembly of valve core and valve housing

Fig. 4 Fabricated damper based on the optimized results from Table 1

translate as changes in stiffness. Fig. 5 shows the vibration test machine, with unbalance rotations, was developed to create vibration amplitude in the system. The developed machine had a test rig that included a fixed frame with two upper and lower plates and four bars. A middle plate was fabricated, which consisted of 4 bushes. An electrical motor also was applied to rotate two unbalanced mass, and thus, the middle plate would experience back and forth motion. Two upper springs were also used to prevent separating the middle plate from four lower springs. Considering M, e, and m as the mass of system, asymmetric eccentricity, and unbalanced mass respectively, characteristics of test machine were M = 85.1 Kg, e = 20.15 mm, and m = 2*1.357 = 2.714 kg. It worth mentioning that the mass of the system is the total mass of vibrating middle plate, motor, and unbalanced mass.

In this system, a three-phase motor to rotate unbalanced weights, an inverter to rotate the motor in constant frequency or frequency sweep, and an inductive displacement sensor that was able to read vibration amplitude were also applied. Because there is an unbalanced mass on the motor axis, the upper plate would start moving up and down in the vertical position as a result of rotation of the motor. Four bars and four bushes are used for constraining this vertical displacement, as Fig. 5 shows.

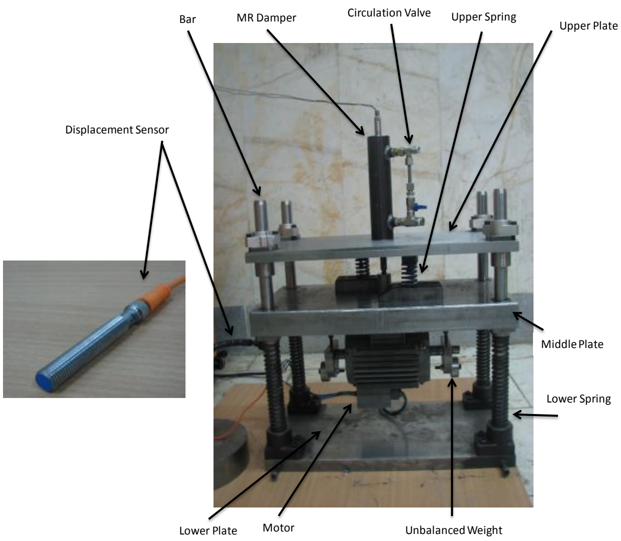

Fig. 5 Fabricated damper and vibration test machine

After the vertical displacement, an inductive displacement sensor would read the displacement. The sensor is fixed in a constant elevation, as Fig. 5 shows. After sensing these amplitudes, the data collected by the sensor would be

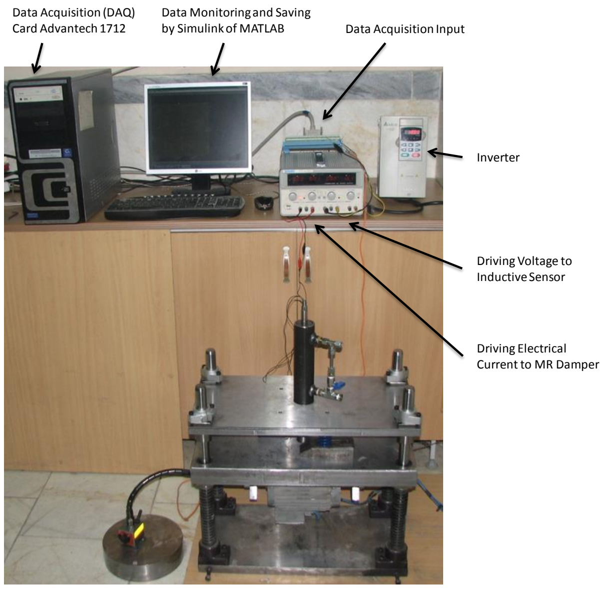

Fig. 6 Developed setup

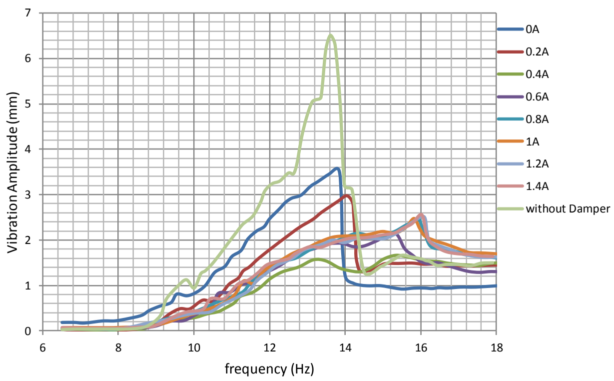

Fig. 7 Vibration amplitude versus frequency in different constant electrical currents

sent to Data Acquisition (DAQ) as Fig. 6 shows. These analog data would be changed to numerical data in DAQ. Finally, those numerical data would be saved in Simulink of MATLAB, and the software would present a graph of those data. Fig. 6 shows the full set-up, MRD, and vibration test machine.

The relationship between frequency and vibration amplitude was examined to find resonant frequency. For monitoring the effect of electrical current, this test was repeated in different constant electrical currents to find the resonant frequency in each constant electrical current. Fig. 7 shows the results of these tests.

These conclusions would be obtained from Fig. 7: first, with increasing the electrical current, resonant frequency would shift to the right since Fig. 7 shows that the crest is moving to the right as electrical current increases. Increasing the value of resonant frequency –as a result of rising applied electrical current- translates as an increase in stiffness because the mass of the system is unchanged. The resonant frequency would change from 13.8 Hz to 16 Hz when the electrical current changes from 0 to 1.4 A. With considering unchanged mass, it represents a significant shift in stiffness; from 640 kN/m to 860 kN/m which shows a substantial shift of -34.37%.

Second, in the resonant area and at electrical currents equal to or less than 0.2 A, damping property would be restored immediately with a low increase in working frequency. This phenomenon is highly likely because of the small effect of MR particles on stiffness when working in low electrical currents. In other words, stiffness in this area experiences minor change, from 640 kN/m to 663 kN/m, which gives the ability to restore its damping property soon.

Third, electrical currents more than 0.8 A do not provide any differences in graphs and the resonance frequency, and thus, stiffness was almost the same in all diagrams. This phenomenon can be caused by saturation of MR in current 0.8 A. Thus, 0.8 A could be called a saturation point of electrical current, after which the electrical current would not be able to make any change in stiffness.

Fourth, as it can be inferred from Fig. 7, the graph does not present a linear relationship between electrical current and vibration amplitude. Even in some areas, the electrical current had reverse effects on damping property. Because of these unknown behaviors, it well worth evaluating this relationship in another test. To examine in detail, in constant frequencies, the relationship between amplitude and electrical current was found. Because in frequencies equal to or lower than 13 Hz, Fig. 7 shows a known and ordinary behavior, the frequency range was divided into two sub-range: frequencies equal to or smaller than 13 Hz and frequencies equal to or more than 14 Hz.

Vibration amplitude as a function of electrical current is shown in Fig. 8 for the lower range. Electrical current varied from 0 to 1.4 A, and different values for vibration amplitude were measured. This test repeated for constant frequencies 9 Hz, 10 Hz, 11 Hz, 12 Hz, and 13 Hz. After 0.9 A, the MRD showed unchanged behavior, and thus, the electrical currents between 0 and 0.9 are shown. As Fig. 8. shows, in all frequencies of the lower sub-range, a reduction in vibration amplitude would be made by increasing electrical current. Because with flowing electrical current, it gives rise to apparent viscosity inside damper, and thus, vibration amplitude would typically decrease. The graph presents a non-linear relationship so that an electrical current about 0.4 A indicates the minimum vibration amplitude. It can be concluded that in this electrical current, the damping force maximized locally. Another phenomenon presented by the graph, an increase in vibration amplitude with rising frequency: it reveals that the system is approaching resonant frequency.

Fig. 9 shows the other range, including upper frequencies. In frequencies of 14 Hz, 15 Hz, 16 Hz, 17 Hz, and 18 Hz, vibration amplitude would increase with giving rise to the electrical current. As it was mentioned, in MRDs by flowing electrical current, the viscosity must increase, and thus, damping force would increase, and finally, the vibrating amplitude would decrease. Nevertheless, the opposite side was seen in this test; with increasing electrical current, vibrating amplitude rises. More likely, the reason for this phenomenon was an increase in system stiffness with increasing current.

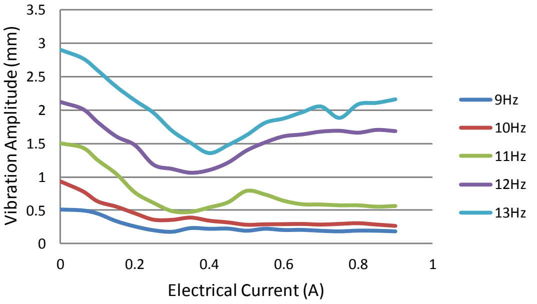

Fig. 8 Vibration amplitude as a function of electrical current in frequencies equal to or lower than 13 Hz

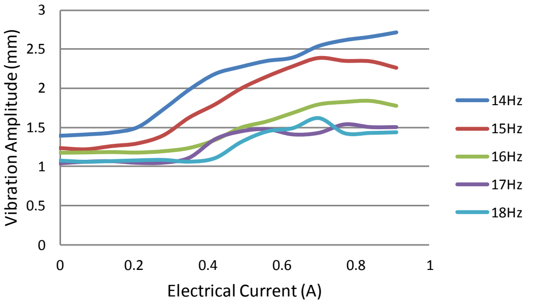

Fig. 9 Vibration amplitude as a function of electrical current in frequencies equal to or more than 14 Hz

4. Conclusions

This study aimed to examine MRDs stiffness shift when applied electrical current increases. An MRD was designed, optimized, and fabricated to achieve proper evaluation. Besides, a vibration test system and a system for circulating MR fluid were also developed. The vibration test machine had a motor and an unbalanced mass to create vibration. For rotating the motor in constant frequency or frequency sweep, an inverter was exploited. For sensing vibration amplitude, an inductive displacement sensor was used. After carrying detailed experimental tests on the fabricated MRD out, the effect of electrical current on stiffness was found. Variation of amplitude and stiffness are functions of applied electrical current, and with increasing the electrical current to the damper, stiffness of system would increase, as well as damping force. More likely, the simultaneous observation of these two variations is because of MR fluid viscoelasticity. Changes in stiffness and damping force with increasing electrical current are not linear. The main conclusion is that with an increase in electrical current from 0 to 1.4 A, resonant frequency would change from 13.8 Hz to 16 Hz, which indicates a change from 640 kN/m to 860 kN/m in stiffness because the mass of the system is unchanged. This shift means the stiffness rose 34.37%. Thus, engineers had better pay close attention to this characteristic. As the future study, this inherent stiffness change would be examined in other MR-based devices and dampers, especially the family of MRDs to which extra parts are added for developing variable stiffness absorber system.

References

Askari, M., Li, J. and Samali, B. (2016), "Semi-active control of smart building-MR damper systems using novel TSK-Inv and max-min algorithms", *Smart Struct. Syst., Int. J.*, **18**(5), 1005-1028. https://doi.org/10.12989/sss.2016.18.5.1005

Behrooz, M., Wang, X. and Gordaninejad, F. (2014), "Modeling of a new semi-active/passive magnetorheological elastomer isolator", *Smart Mater. Struct.*, **23**(4), 045013. https://doi.org/10.1088/0964-1726/23/4/045013

Deng, H.X., Gong, X.L. and Wang, L.H. (2006), "Development of an adaptive tuned vibration absorber with magnetorheological elastomer", *Smart Mater. Struct.*, **15**(5), 111-116. https://doi.org/10.1088/0964-1726/15/5/N02

Jugulkar, L.M., Singh, S. and Sawant, S.M. (2016), "Analysis of suspension with variable stiffness and variable damping force for automotive applications", *Adv. Mech. Eng.*, **8**(5), 1-19. https://doi.org/10.1177%2F1687814016648638

Li, W., Wang, X.Y., Zhang, X.Z. and Zhou, Y. (2009), "Development and analysis of a variable stiffness damper using an MR bladder", *Smart Mater. Struct.*, **18**(7), 074007. https://doi.org/10.1088/0964-1726/18/7/074007

Liu, Y., Matsuhisa, H., Utsuno, H. and Park, J.G. (2006), "Vibration control by a variable damping and stiffness system with magnetorheological dampers", *JSME Int. J. Series C Mech. Syst. Mach. Eleme. Manuf.*, **49**(2), 411-417. https://doi.org/10.1299/jsmec.49.411

Maddah, A.A., Hojjat, Y., Karafi, M.R. and Ashory, M.R. (2017), "Reduction of magneto rheological damper stiffness by incorporating of an eddy current damper", *J. Sound Vib.*, **396**, 51-68. https://doi.org/10.1016/j.jsv.2017.02.011

Sun, C., Nagarajaiah, S. and Dick, A.J. (2014a), "Family of smart tuned mass dampers with 2 variable frequency under harmonic excitations and ground motions: Closed-form evaluation", *Smart Struct. Syst., Int. J.*, **13**(2), 319-341. https://doi.org/10.12989/sss.2014.13.2.319

Sun, S., Deng, H. and Li, W. (2014b), "A variable stiffness and damping suspension system for trains", *Proceedings of SPIE: Active and Passive Smart Structures and Integrated Systems*, **9057**, 1-9. https://doi.org/10.1117/12.2045023

Sun, S., Yang, J., Li, W., Deng, H., Du, H. and Alici, G. (2015), "Development of a novel variable stiffness and damping magnetorheological fluid damper", *Smart Mater. Struct.*, **24**(8), 085021-1-085021-10. https://doi.org/10.1088/0964-1726/24/8/085021

Sun, S., Tang, X., Li, W. and Du, H. (2017), "Advanced vehicle suspension with variable stiffness and damping MR damper", *Proceedings of 2017 IEEE International Conference on Mechatronics (ICM)*, Churchill, Australia. https://doi.org/10.1109/ICMECH.2017.7921148

Wang, X., Pereira, E., Díaz, I.M. and García-Palacios, J.H. (2018), "Velocity feedback for controlling vertical vibrations of pedestrian-bridge crossing. Practical guidelines", *Smart Struct. Syst., Int. J.*, **22**(1), 95-103. https://doi.org/10.12989/sss.2018.22.1.095

Weber, F., Boston, C. and Maślanka, M. (2010), "An adaptive tuned mass damper based on the emulation of positive and negative stiffness with an MRD", *Smart Mater. Struct.*, **20**, 015012. https://doi.org/10.1088/0964-1726/20/1/015012

Zhu, X., Deng, L., Sun, S., Yan, T., Yu, J., Ma, Z. and Li, W. (2019), "Development of a variable stiffness magnetorheological damper with self-powered generation capability", *J. Intel. Mater. Syst. Struct.*, **31**(2), 209-219. https://doi.org/10.1177/1045389x19862640

CC